JACS
JOURNAL OF THE AMERICAN CHEMICAL SOCIETY
Communication
pubs.acs.org/JACS

Ligand-Stabilized $Au_{13}Cu_x$ (x = 2, 4, 8) Bimetallic Nanoclusters: Ligand Engineering to Control the Exposure of Metal Sites

Huayan Yang,[†] Yu Wang,[†] Jing Lei,[†] Lei Shi,[‡] Xiaohu Wu,[‡] Ville Mäkinen,[§] Shuichao Lin,[†] Zichao Tang,[‡] Jian He,[∥] Hannu Häkkinen,[§] Lansun Zheng,[†] and Nanfeng Zheng*[,†]

[†]State Key Laboratory for Physical Chemistry of Solid Surfaces, Collaborative Innovation Center of Chemistry for Energy Materials, and Department of Chemistry, College of Chemistry and Chemical Engineering, Xiamen University, Xiamen 361005, China

[‡]State Key Laboratory of Molecular Reaction Dynamics, Dalian Institute of Chemical Physics, Chinese Academy of Sciences, Dalian 116023, China

[§]Departments of Physics and Chemistry, Nanoscience Center, University of Jyväskylä, FI-40014 Jyväskylä, Finland

[∥]Institute of Physics and Mechanical and Electrical Engineering, Xiamen University, Xiamen 361005, China

Supporting Information

ABSTRACT: Three novel bimetallic Au-Cu nanoclusters stabilized by a mixed layer of thiolate and phosphine ligands bearing pyridyl groups are synthesized and fully characterized by X-ray single crystal analysis and density functional theory computations. The three clusters have an icosahedral Au_{13} core face-capped by two, four, and eight Cu atoms, respectively. All face-capping Cu atoms in the clusters are triply coordinated by thiolate or pyridyl groups. The surface ligands control the exposure of Au sites in the clusters. In the case of the $Au_{13}Cu_8$ cluster, the presence of 12 2-pyridylthiolate ligands still leaves open space for catalysis. All the 3 clusters are 8-electron superatoms displaying optical gaps of 1.8−1.9 eV. The thermal decomposition studies suggest that the selective release of organic ligands from the clusters is possible.

Since the development of the Brust synthesis in 1994,[1] thiol-stabilized metal nanoparticles are a class of stable metal nanomaterials that have found applications in many areas, such as biology, sensing, nanotechnology and catalysis.[2−7] For many applications, the fine-tuning of composition and surface modification of the metal nanoparticles is important.[4,5] Understanding the interfacial structure between metal core and thiol ligands is thus crucial. With the structure determination of several Au nanoclusters (i.e., Au_{102},[8] Au_{25},[9,10] Au_{38},[11] and Au_{36}[12]) by X-ray single crystal analysis, the past several years have witnessed significant progress toward understanding the interfacial structure of thiolated Au nanoclusters. It is found that $RS(AuSR)_x$ (x = 1, 2) oligomeric units are commonly present on the surface of thiolated Au nanoclusters.[13−15] Based on such motif, various structures of thiolated Au and even Ag containing nanoclusters have been computationally predicted.[16−28] Au_{25} and Au_{38} represent the most successful examples whose structures were predicted[18−20] and later experimentally confirmed.[9−11]

However, modification of the metal-ligand interface of stabilized gold nanoclusters to display other structural units than $RS(AuSR)_x$ may require the use of nonthiolate ligands and other metals than gold. Taking thiolated Au_{25} as an example, its structure is essentially an Au_{13} icosahedral cluster face-capped by 12 Au atoms. An Au_{13} icosahedron has 20 triangular Au_3 faces. Structurally, the number of metal atoms face-capping the triangular Au_3 faces could be varied from 0 to 20. Very recently, we have found that thiolated Ag nanoclusters do not necessarily have $RS(MSR)_x$ units on their surfaces due to the following two structural features:[29,30] (1) Surface Ag atoms do not need to take the linear bicoordination; and (2) when coordinated to Ag, thiolate can bridge more than two metal atoms. We thus believe that the combined use of Au and other metals would significantly enrich the structure of thiolated Au-containing nanoclusters. The goal of this work was to prepare thiolated metal nanoclusters containing Au_{13} icosahedron with <12 triangular Au_3 faces capped by metal atoms. The achievement of this goal would eventually provide an effective way to tune the electronic properties and expose different number of Au sites for catalysis.

We report our success in preparing three Au-Cu bimetallic nanoclusters, $Au_{13}Cu_2$, $Au_{13}Cu_4$ and $Au_{13}Cu_8$, having icosahedral Au_{13} core decorated by two, four, and eight Cu atoms, respectively. The total structures of the three clusters were determined by X-ray single-crystal analysis. The number of face-capping Cu atoms is determined by the available binding sites offered by the 12 surface ligands. The surface ligands also control the exposure of Au sites in the clusters and thus their catalysis. Density functional theory (DFT) calculations were used to explain the stability of the clusters, analyze the electronic structure in terms of the superatom model,[31] and correlate the electronic structure to the measured UV/vis absorption spectra.

The syntheses of $Au_{13}Cu_2$ and $Au_{13}Cu_4$ involved the chemical reduction of Au and Cu species by $NaBH_4$ using a two-phase method in the presence of both thiol and phosphine as surface capping ligands (see Supporting Information (SI) for details). X-ray single crystal analysis reveals that $Au_{13}Cu_2$ and $Au_{13}Cu_4$ are crystallized in monoclinic space groups P-1, and $C2/c$, respectively. As illustrated in Figure 1, the compositions of $Au_{13}Cu_2$ and $Au_{13}Cu_4$ clusters are $[Au_{13}Cu_2(PPh_3)_6(SPy)_6]^+$ (Py = 2-pyridyl) and $[Au_{13}Cu_4(PPh_2Py)_4(SC_6H_4\text{-}tert\text{-}C_4H_9)_8]^+$. Both $Au_{13}Cu_2$ and $Au_{13}Cu_4$ have an icosahedral Au_{13} as their

Received: March 4, 2013
Published: June 18, 2013

dx.doi.org/10.1021/ja402249s | J. Am. Chem. Soc. 2013, 135, 9568−9571

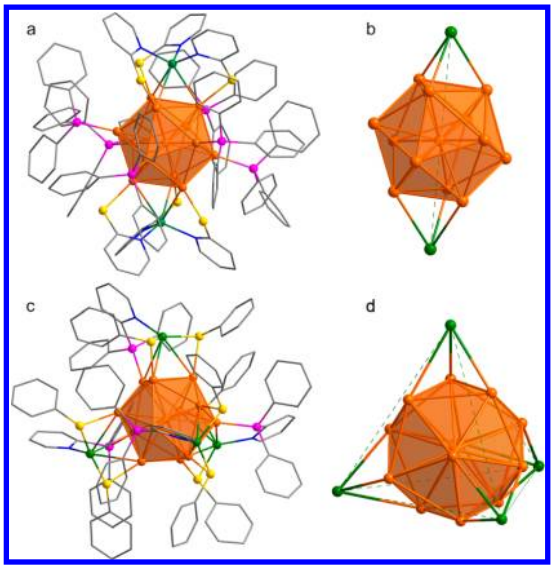

Figure 1. Crystal structures of $[Au_{13}Cu_2(PPh_3)_6(SPy)_6]^+$ (a,b) and $[Au_{13}Cu_4(PPh_2Py)_4(SC_6H_4\text{-}tert\text{-}C_4H_9)_8]^+$ (c,d) clusters. (b,d) Structures showing only metal atoms. Color legend: gold sphere, Au; green sphere, Cu; yellow sphere, S; pink sphere, P; gray stick, C; blue stick, N. All H atoms in both clusters and *tert*-butyl groups in $[Au_{13}Cu_4(PPh_2Py)_4(SC_6H_4\text{-}tert\text{-}C_4H_9)_8]^+$ are omitted for clarity.

core, similar to the reported $Au_{25}(SR)_{18}^-$ clusters. It should be noted that although doping Au_{13} clusters with other metals (e.g., Pd, Pt, Ag, Cu) has been well-documented,[32−34] it still remains challenging to decorate the outer surface of Au_{13} clusters with nongold metal atoms to form well-defined bimetallic clusters. An Au_{13} icosahedron has 20 triangular Au_3 faces. In the reported $Au_{25}(SR)_{18}^-$ cluster, 12 of the 20 Au_3 faces are face-capped by Au atoms. In $Au_{13}Cu_2$, the Au_{13} core is face-capped by only two Cu (Figure 1b). The two Cu atoms in $Au_{13}Cu_2$ are oriented along one of the 3-fold axes of the icosahedral Au_{13} with Au-Cu distances between 2.775 and 2.886 Å (averaged at 2.824 Å). In comparison, each $Au_{13}Cu_4$ has the Au_{13} core face-capped by four Cu atoms (Figure 1d). The four Cu atoms in each $Au_{13}Cu_4$ are located in a tetrahedral configuration with Au-Cu distances between 2.785 and 3.165 Å (averaged at 2.973 Å). In the Au_{13} core of $Au_{25}(SR)_{18}^-$ cluster, it should be noted that the average Au-Au distance from the central atom to the surrounding 12 Au atoms is ∼3.8% shorter than the Au-Au distance (∼2.884 Å) in bulk Au. Such a structural feature of Au-Au bond contraction is also revealed in $Au_{13}Cu_2$ and $Au_{13}Cu_4$, although their Au_{13} cores are capped by different numbers of Cu atoms. In the Au_{13} cores of $Au_{13}Cu_2$ and $Au_{13}Cu_4$, the Au-Au distances from the central atom are averaged at 2.771 and 2.757 Å, respectively. Compared with bulk Au, up to 4.4% of Au-Au contraction is observed in $Au_{13}Cu_4$.

The presence of $RS(AuSR)_x$ (x = 1, 2) units is always revealed in the determined structures of thiolated Au nanoclusters. However, such structural units are not present in $Au_{13}Cu_2$ and $Au_{13}Cu_4$ (Figure 1a,c). In both clusters, all of the 12 outer Au atoms of the Au_{13} core are passivated by either a phosphine or a thiolate ligand. In $Au_{13}Cu_2$, the Au_{13} icosahedron is passivated by six PPh_3 and six 2-pyridinethiolates. The six PPh_3 ligands coordinate (one each) in a radial fashion to the six gold atoms that are arranged in cyclohexane-like 'chair' configuration at the 'equatorial' positions of the Au_{13} core, similar to the structure in $[(Ph_3P)_6Au_6Ag_6Pt(AgI_3)_2]$.[35] In an Au_{13} icosahedron, the cyclohexane-like unit is capped on top and below by two Au_3 triangles. As bidentate ligands, the six 2-pyridylthiolate ligands

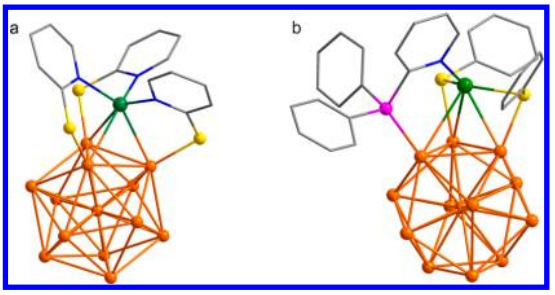

Figure 2. Local coordination structures of Cu atom in $[Au_{13}Cu_2(PPh_3)_6(SPy)_6]^+$ (a) and $[Au_{13}Cu_4(PPh_2Py)_4(SC_6H_4\text{-}tert\text{-}C_4H_9)_8]^+$ (b). Color legend: gold sphere, Au; green sphere, Cu; yellow sphere, S; pink sphere, P; gray stick, C; blue stick, N.

(one each) bind to the six Au atoms from the two Au_3 triangles, leaving six pyridyl motifs available to hold two Cu atoms at the opposite sides of the cluster. Each Cu in $Au_{13}Cu_2$ is thus coordinated by three pyridyl groups (Figure 2a). In comparison, the surface Au atoms of the Au_{13} unit in $Au_{13}Cu_4$ are protected by four PPh_2Py and eight 4-*tert*-butylbenzenthiol ligands. Both thiol and PPh_2Py serve as bidentate ligands. While every PPh_2Py binds to Au using its P site and Cu using its pyridyl motif, each 4-*tert*-butyl-benzenthiolate is doubly bridged between Au and Cu atoms. In $Au_{13}Cu_4$, each Cu capping on the Au_{13} core is triply bound by two thiolate motifs and by one pyridyl (Figure 2b). The triple coordination of Cu atoms in both $Au_{13}Cu_2$ and $Au_{13}Cu_4$ is quite different from those for the Ag atoms tethered to the underlying M_3 facets found in phosphine-capped $Au_{18}Ag_{20}$ and $Au_{18}Ag_{19}$ clusters.[36,37] The tethered Ag sites in those two clusters are tetrahedrally coordinated by four halide anions.

In short, $Au_{13}Cu_2$ and $Au_{13}Cu_4$ have the following two common structural features: (1) There are a total number of 12 phosphine and thiolate ligands binding to the 12 apex sites of the icosahedral Au_{13} core through Au-P and Au-S interactions; and (2) Cu atoms are face-capping triangular Au_3 faces of the Au_{13} core and tricoordinated by three pyridyl/thiolate motifs. The number of face-capping Cu atoms depends on the available coordination motifs from the 12 surface ligands. In $Au_{13}Cu_2$, the binding of six PPh_3 and six 2-pyridinethiolate ligands on Au_{13} leads to six pyridyl motifs available for Cu. Such a ligand arrangement yields two positions to hold face-capping Cu atoms on the Au_{13} core. In $Au_{13}Cu_4$, however, the binding of four PPh_2Py and eight 4-*tert*-butyl-benzenthiolate ligands leaves 12 pyridyl and thiolate coordinating motifs available for holding four surface-capping Cu atoms.

Based on the above structural analysis on $Au_{13}Cu_2$ and $Au_{13}Cu_4$, it is expected that the bimetallic Au-Cu nanocluster with Au_{13} core face-capped by different number of Cu atoms can be prepared by changing the surface ligands appropriately. Experimentally, we have thus attempted to prepare Au-Cu nanoclusters with more face-capping Cu atoms. By increasing the Cu/Au ratio and using 2-pyridinethiol in the synthesis, we successfully prepared $[Au_{13}Cu_8(PPh_2Py)_{12}]^+$ cluster ($Au_{13}Cu_8$) having Au_{13} core face-capped by eight Cu atoms (Figure 3a). In each $Au_{13}Cu_8$, the eight Cu atoms are divided into two groups (Figure3b), two oppositely oriented single Cu atoms across the Au_{13} core (Au-Cu averaged at 2.768 Å) and three equatorially distributed Cu_2 dimers (Au-Cu averaged at 2.911 Å). In the Au_{13} cores of $Au_{13}Cu_8$, the Au-Au distances from the central atom are averaged at 2.768 Å. The Au_{13} unit is capped by 12 2-pyridylthiolate ligands. Each 2-pyridylthiolate in $Au_{13}Cu_8$ binds to one Au through Au-S and two Cu atoms through Cu-S and

dx.doi.org/10.1021/ja402249s | J. Am. Chem. Soc. 2013, 135, 9568−9571

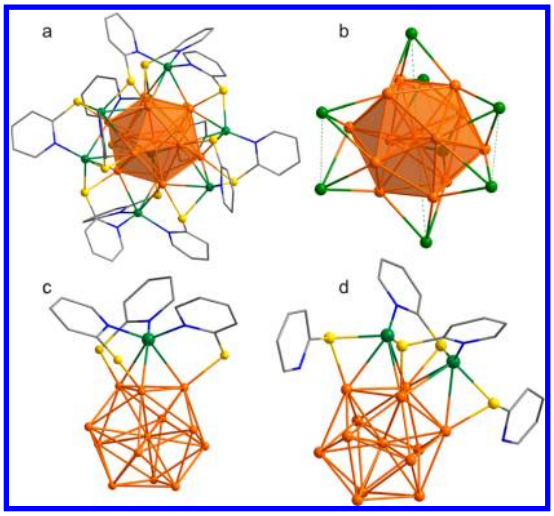

Figure 3. Crystal structure of $[Au_{13}Cu_8(PPh_2Py)_{12}]^+$. (a) Overall structure; (b) Distribution of eight Cu atoms on Au_{13}; (c,d) Local coordination structures of two types of Cu atoms in $[Au_{13}Cu_8(PPh_2Py)_{12}]^+$. Color legend: gold sphere, Au; green sphere, Cu; yellow sphere, S; gray stick, C; blue stick, N. All H atoms are omitted for clarity.

Cu-N, resulting in 24 binding sites (12 thiolates and 12 pyridyls) available to have 8 Cu atoms face-capping the Au_{13} core. As shown in Figure 3c,d, while each of the two oppositely oriented Cu atoms is coordinated by three pyridyls, each of the six Cu atoms that are equatorially distributed are coordinated by two thiolates and one 2-pyridyl.

As identified by the X-ray single-crystal analysis, each $Au_{13}Cu_4$ cluster has a +1 charge which is balanced by a ClO_4^- counteranion. ClO_4^- anions are located in the voids between the clusters (Figure S1). Since each Au ($5d^{10}6s^1$) or Cu ($3d^{10}4s^1$) has one valence electron and the bonding to each thiolate anion consumes one valence electron, each $Au_{13}Cu_4$ cluster has 8 ($17 \times 1\text{-}8 \times 1\text{-}1$) electrons and obeys the superatom rule.[31,38] Unfortunately, the unambiguous identification of counteranions in the single crystals of $Au_{13}Cu_2$ and $Au_{13}Cu_8$ was not possible, probably due to the heavy disordering of the anions. For this reason, we have performed mass spectrometry (ESI-MS) measurements to evaluate the charge state of $Au_{13}Cu_2$ and $Au_{13}Cu_8$. Both $Au_{13}Cu_2$ and $Au_{13}Cu_8$ were found to have a +1 charge and display clean and well-resolved peaks at 4922.3 and 4390.8 m/z under positive ion mode, respectively (Figure S2).

DFT analysis of the atomic structure and charges and electronic structure (Table S1 and Figures S3–S5) shows unambiguously that $Au_{13}Cu_2$, $Au_{13}Cu_4$, and $Au_{13}Cu_8$ clusters are most stable as charged cations when all the systems are 8-electron superatoms. The clusters have significant calculated HOMO-LUMO gaps (of the order of 1–1.3 eV). While the P-superatom orbitals are always fully occupied, they are in many cases close in energy and partially mixed with hybridized Cu^+/ligand states. The degree of Cu^+/ligand mixing increases from $x = 2$ to 8. The superatom D orbitals are found either as LUMO states or close to the LUMO states. $Au_{13}Cu_4$ appears as a special case where both HOMO and LUMO states show strong hybridization of Cu^+/ligand contributions. The strong interaction between Cu^+ and nitrogen of the pyridyl ring is similar to coordination to benzotriazolate (BTA), which has been previously discussed in context of small copper clusters and Cu(111) surface protected by BTA-Cu-BTA units.[39,40] Our interpretation is thus that Cu^+ is part of the ligand layer.

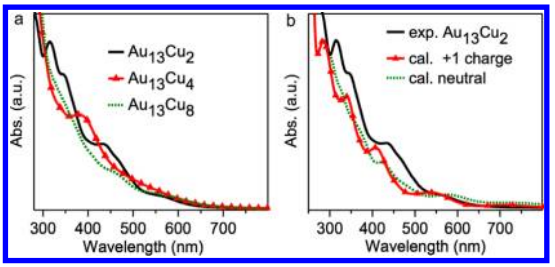

Figure 4. (a) UV/vis absorption spectra of $Au_{13}Cu_2$, $Au_{13}Cu_4$ and $Au_{13}Cu_8$ in CH_2Cl_2. (b) Comparison of the measured spectra of $Au_{13}Cu_2$ with the theoretical absorption spectra calculated from the LR-TDDFT. The spectra were calculated both for cationic and neutral clusters. In the calculated spectra the individual optical transitions have been smeared out by Gaussians of 0.075 eV width and the intensity is scaled to correspond to the experiment at around 550 nm.

As shown in Figure 4, our UV/vis spectral measurements reveal that $Au_{13}Cu_2$, $Au_{13}Cu_4$, and $Au_{13}Cu_8$ in CH_2Cl_2 exhibit UV/vis absorption spectra with molecule-like optical transitions. The optical gaps for $Au_{13}Cu_2$, $Au_{13}Cu_4$ and $Au_{13}Cu_8$ are estimated from the measured absorption edge and are 1.88, 1.87, and 1.80 eV, respectively. Comparison of the computed spectra for neutral and cationic $Au_{13}Cu_2$ to the measured spectrum shows that the calculated spectrum for the cationic $Au_{13}Cu_2$ is in a very good agreement with the measured one, reproducing all the four observed features in the experimental data, while the spectrum of the neutral $Au_{13}Cu_2$ does not correspond to the experiment. Theory thus gives strong support for the cationic state of $Au_{13}Cu_2$. Furthermore, the average Au-Cu distance in the computationally optimized cationic $Au_{13}Cu_2$ cluster corresponds much better to the measured value as compared to the neutral $Au_{13}Cu_2$.

Having different surface ligands should create different chemical properties among the three obtained bimetallic Au-Cu nanoclusters. For example, compared with PPh_3, PPh_2Py and *tert*-C_4H_9-$C_6H_4S^-$, the size of 2-pyridylthiolate is smaller. As clearly illustrated in their space-filling structures (Figure S6), the presence of 12 2-pyridylthiolate ligands on the surface of $Au_{13}Cu_8$ still leaves open space for small molecules to access its Au sites. In comparison, the surface ligands on $Au_{13}Cu_2$ and $Au_{13}Cu_4$ completely block the Au sites for catalysis applications. Experimentally, the hydrogenation of 4-nitrophenol by $NaBH_4$ to 4-aminophenol was chosen as a model reaction to evaluate the accessibility of Au sites in the three clusters. The reduction process was monitored by UV/vis absorption spectroscopy (Figure S7). As shown in the reduction processes, in the presence of $Au_{13}Cu_8$, the intensity of the absorption peak of 4-nitrophenol at 400 nm quickly decreased, and the absorption of 4-aminophenol at 295 nm increased accordingly. The reduction of 4-nitrophenol into 4-aminophenol was completed in 10 min with the color change of bright yellow to colorless. A linear relation of $\ln(C_t/C_0)$ vs time, where C_t and C_0 are 4-nitrophenol concentrations at time t and 0, respectively, was observed. In comparison, in the presence of $Au_{13}Cu_2$ or $Au_{13}Cu_4$ clusters, the reactions did not proceed. Moreover, carbon nanotube-supported $Au_{13}Cu_8$ clusters were also catalytically active in the aerobic selective oxidation of benzyl alcohol, while $[Au_{25}(SC_2H_4C_6H_5)_{18}]^-$ clusters without removal of surface ligands displayed negligible catalysis in the same reaction (Table S2).

Considering the copresence of phosphine and thiolate on the surface of $Au_{13}Cu_2$ and $Au_{13}Cu_4$, thermal gravimetric analysis (TGA) was also performed to investigate the thermal

dx.doi.org/10.1021/ja402249s | J. Am. Chem. Soc. 2013, 135, 9568–9571

degradation characteristics of the ligands. TGA curves (in N_2) of $Au_{13}Cu_2$ and $Au_{13}Cu_4$ show major weight losses between 200 and 325 °C (Figure S8). Two distinguishable weight losses before and after 270 °C were observed on $Au_{13}Cu_4$, suggesting that the surface ligands on $Au_{13}Cu_4$ undergo stepwise thermal degradation. To further investigate how the ligands were thermally degraded from $Au_{13}Cu_4$, the thermal decomposition products were analyzed using a high-resolution time-of-flight mass spectrometer (see SI for details). These thermal decomposition studies suggested that the selective removal of surface ligands is possible for metal nanoclusters cocapped by two different types of ligands.

The removal of organic ligands from clusters would make it possible to create more empty Au sites available for catalysis. CNT-supported $Au_{13}Cu_8$ clusters treated at 370 °C under vacuum readily serve as a more active catalyst than pure Au_{25} clusters in the aerobic selective oxidation of benzyl alcohol. Under 5 atm O_2 at 80 °C, the treated $Au_{13}Cu_8$ clusters gave a benzyl alcohol conversion of 46.9% with 61.0% selectivity to benzyl aldehyde (Table S2). In comparison, the conversion of benzyl alcohol achieved by the treated Au_{25} clusters was 33.2% under the same conditions, suggesting an important role of heteroatom doping in enhancing catalysis by metal nanoclusters.

To summarize, by the combined use of thiol and phosphine ligands, one of which bears a pyridyl group, three bimetallic Au-Cu nanoclusters ($Au_{13}Cu_2$, $Au_{13}Cu_4$, $Au_{13}Cu_8$) were synthesized and structurally characterized by X-ray single-crystal analysis. All clusters have icosahedral Au_{13} as their core decorated with two, four, or eight Cu atoms which are tricoordinated by pyridyl/thiolate groups. The number of surface capping Cu atoms is determined by the available coordinating sites offered by the surface ligands. The ligand engineering controls the exposure of Au sites in the clusters. All clusters are +1 charged 8-electron superatoms as confirmed by DFT calculations. The thermal decomposition investigations indicate that the selective release of organic ligands from the clusters is possible. Moreover, based on the structural feature of bimetallic nanoclusters reported in this work, more thiolated bimetallic nanoclusters with Au_{13} core face-capped by different number of metal atoms are expected to be prepared by tuning surface organic ligands.

■ ASSOCIATED CONTENT

Ⓢ Supporting Information

Experimental details and crystallographic data. This material is available free of charge via the Internet at http://pubs.acs.org.

■ AUTHOR INFORMATION

Corresponding Author

nfzheng@xmu.edu.cn

Notes

The authors declare no competing financial interest.

■ ACKNOWLEDGMENTS

We thank MOST of China (2011CB932403, 2011CB201301, 2009CB930703), the NSFC (21227001, 21131005, 21021061, 20925103, 20923004), the Fundamental Research Funds for the Central Universities (2010121042) for the financial support. The computational work is supported by the Academy of Finland, and the computations were made in NSC (Jyväskylä) and in HLRS (Stuttgart). V.M. and H.H. wish to thank L. Lehtovaara for his help in the LR-TDDFT calculations.

■ REFERENCES

(1) Brust, M.; Walker, M.; Bethell, D.; Schiffrin, D. J.; Whyman, R. *J. Chem. Soc., Chem. Commun.* **1994**, 801.
(2) Daniel, M.-C.; Astruc, D. *Chem. Rev.* **2003**, *104*, 293.
(3) Astruc, D.; Lu, F.; Aranzaes, J. R. *Angew. Chem., Int. Ed.* **2005**, *44*, 7852.
(4) Niemeyer, C. M. *Angew. Chem., Int. Ed.* **2001**, *40*, 4128.
(5) Templeton, A. C.; Wuelfing, W. P.; Murray, R. W. *Acc. Chem. Res.* **1999**, *33*, 27.
(6) Tsukuda, T. *Bull. Chem. Soc. Jpn.* **2012**, *85*, 151.
(7) Zheng, N. F.; Stucky, G. D. *J. Am. Chem. Soc.* **2006**, *128*, 14278.
(8) Jadzinsky, P. D.; Calero, G.; Ackerson, C. J.; Bushnell, D. A.; Kornberg, R. D. *Science* **2007**, *318*, 430.
(9) Heaven, M. W.; Dass, A.; White, P. S.; Holt, K. M.; Murray, R. W. *J. Am. Chem. Soc.* **2008**, *130*, 3754.
(10) Zhu, M. Z.; Aikens, C. M.; Hollander, F. J.; Schatz, G. C.; Jin, R. C. *J. Am. Chem. Soc.* **2008**, *130*, 5883.
(11) Qian, H. F.; Eckenhoff, W. T.; Zhu, Y.; Pintauer, T.; Jin, R. C. *J. Am. Chem. Soc.* **2010**, *132*, 8280.
(12) Zeng, C. J.; Qian, H. F.; Li, T.; Li, G.; Rosi, N. L.; Yoon, B.; Barnett, R. N.; Whetten, R. L.; Landman, U.; Jin, R. C. *Angew. Chem., Int. Ed.* **2012**, *51*, 13114.
(13) Häkkinen, H. *Nat Chem* **2012**, *4*, 443.
(14) Qian, H. F.; Zhu, M. Z.; Wu, Z. K.; Jin, R. C. *Acc. Chem. Res.* **2012**, *45*, 1470.
(15) Pei, Y.; Zeng, X. C. *Nanoscale* **2012**, *4*, 4054.
(16) Häkkinen, H.; Walter, M.; Grönbeck, H. *J. Phys. Chem. B* **2006**, *110*, 9927.
(17) Chaki, N. K.; Negishi, Y.; Tsunoyama, H.; Shichibu, Y.; Tsukuda, T. *J. Am. Chem. Soc.* **2008**, *130*, 8608.
(18) Akola, J.; Walter, M.; Whetten, R. L.; Häkkinen, H.; Grönbeck, H. *J. Am. Chem. Soc.* **2008**, *130*, 3756.
(19) Lopez-Acevedo, O.; Tsunoyama, H.; Tsukuda, T.; Hakkinen, H.; Aikens, C. M. *J. Am. Chem. Soc.* **2010**, *132*, 8210.
(20) Pei, Y.; Gao, Y.; Zeng, X. C. *J. Am. Chem. Soc.* **2008**, *130*, 7830.
(21) Pei, Y.; Gao, Y.; Shao, N.; Zeng, X. C. *J. Am. Chem. Soc.* **2009**, *131*, 13619.
(22) Jiang, D. E.; Tiago, M. L.; Luo, W. D.; Dai, S. *J. Am. Chem. Soc.* **2008**, *130*, 2777.
(23) Lopez-Acevedo, O.; Akola, J.; Whetten, R. L.; Gronbeck, H.; Häkkinen, H. *J. Phys. Chem. C* **2009**, *113*, 5035.
(24) Malola, S.; Häkkinen, H. *J. Phys. Chem. Lett.* **2011**, *2*, 2316.
(25) Pei, Y.; Pal, R.; Liu, C. Y.; Gao, Y.; Zhang, Z. H.; Zeng, X. C. *J. Am. Chem. Soc.* **2012**, *134*, 3015.
(26) Jiang, D. E. *Chem.—Eur. J.* **2011**, *17*, 12289.
(27) Jiang, D.-e.; Walter, M.; Akola, J. *J. Phys. Chem. C* **2010**, *114*, 15883.
(28) Negishi, Y.; Iwai, T.; Ide, M. *Chem. Commun.* **2010**, *46*, 4713.
(29) Yang, H. Y.; Lei, J.; Wu, B. H.; Wang, Y.; Zhou, M.; Xia, A. D.; Zheng, L. S.; Zheng, N. F. *Chem. Commun.* **2013**, *49*, 300.
(30) Yang, H. Y.; Wang, Y.; Zheng, N. F. *Nanoscale* **2013**, *5*, 2674.
(31) Walter, M.; Akola, J.; Lopez-Acevedo, O.; Jadzinsky, P. D.; Calero, G.; Ackerson, C. J.; Whetten, R. L.; Gronbeck, H.; Häkkinen, H. *Proc. Natl. Acad. Sci. U.S.A.* **2008**, *105*, 9157.
(32) Copley, R. C. B.; Mingos, D. M. P. *J. Chem. Soc., Dalton Trans.* **1996**, 491.
(33) Laupp, M.; Strähle, J. *Angew. Chem., Int. Ed.* **1994**, *33*, 207.
(34) Teo, B. K.; Zhang, H.; Shi, X. *J. Am. Chem. Soc.* **1993**, *115*, 8489.
(35) Teo, B. K.; Zhang, H. *J. Organomet. Chem.* **2000**, *614-615*, 66.
(36) Teo, B. K.; Zhang, H.; Shi, X. *J. Am. Chem. Soc.* **1990**, *112*, 8552.
(37) Teo, B. K.; Hong, M. C.; Zhang, H.; Huang, D. B. *Angew. Chem., Int. Ed.* **1987**, *26*, 897.
(38) Häkkinen, H. *Chem. Soc. Rev.* **2008**, *37*, 1847.
(39) Salorinne, K.; Chen, X.; Troff, R. W.; Nissinen, M.; Häkkinen, H. *Nanoscale* **2012**, *4*, 4095.
(40) Chen, X.; Häkkinen, H. *J. Phys. Chem. C* **2012**, *116*, 22346.